Structural Monitoring and Maintenance, *Vol. 2, No. 3 (2015) 213-236*
DOI: http://dx.doi.org/10.12989/smm.2015.2.3.213

Mode conversion and scattering analysis of guided waves at delaminations in laminated composite beams

Reza Soleimanpour and Ching-Tai Ng*

School of Civil, Environmental and Mining Engineering, The University of Adelaide, SA 5005, Australia

(Received March 3, 2015, Revised August 17, 2015, Accepted August 27, 2015)

Abstract. The paper presents an investigation into the mode conversion and scattering characteristics of guided waves at delaminations in laminated composite beams. A three-dimensional (3D) finite element (FE) model, which is experimentally verified using data measured by 3D scanning laser vibrometer, is used in the investigation. The study consists of two parts. The first part investigates the excitability of the fundamental anti-symmetric mode (A_0) of guided wave in laminated composite beams. It is found that there are some unique phenomena, which do not exist for guided waves in plate structures, make the analysis become more complicated. The phenomena are observed in numerical study using 3D FE simulations. In the second part, several delaminated composite beams are studied numerically to investigate the mode conversion and scattering characteristics of the A_0 guided wave at delaminations. Different sizes, locations and through-thickness locations of the delaminations are investigated in detail. The mode conversion and scattering phenomena of guided waves at the delaminations are studied by calculating reflection and transmission coefficients. The results show that the sizes, locations and through-thickness locations of the delaminations have significant effects on the scattering characteristics of guided waves at the delaminations. The results of this research would provide better understanding of guided waves propagation and scattering at the delaminations in the laminated composite beams, and improve the performance of guided wave damage detection methods.

Keywords: laminated composite beam; finite element; delamination; guided waves; mode conversion; scattering; laser vibrometer

1. Introduction

The applications of fibre-reinforced composite materials, such as carbon fibre-epoxy laminates, have substantially increased in various fields, such as civil structures, military, mechanical engineering and aerospace over the past few years. Fibre-reinforced composite materials have some attractive properties, such as high stiffness, lightweight and corrosion resistance, which make them as a suitable choice for engineering applications. However, they are vulnerable to certain types of damages and are likely to encounter a wide variety of complex issues when they are subjected to impact and fatigue. Delamination is one of the most common types of damages in composite materials. It significantly reduces the compressive strength and stiffness, which results in major structural damages or even structural failure.

*Corresponding author, Senior Lecturer, E-mail: alex.ng@adelaide.edu.au

http://www.techno-press.org/?journal=smm&subpage=7 ISSN: 2288-6605 (Print), 2288-6613 (Online)

In recent years, guided wave techniques, have received considerable attention due to their efficiency in detecting structural flaws (Alleyne and Cawley 1991, Staudenmann 1995, Zhu *et al*. 1998, Lowe and Diligent 2002, Ng *et al.* 2009, Veidt and Ng 2011, Ng 2015). The approach employs mechanical stress waves that propagate in structures and guided by structural boundaries, to detect the damages. One of the advantages of guided waves is that it can travel a long distance with a very little loss in energy, which means guided waves can be used in safety inspection for a large area of the structures. Nowadays, guided waves techniques have been widely used for damage detection in a wide range of engineering structures, such as pipelines, aircrafts, railways and bridges (Rose and Soley 2000, Hongerholt *et al.* 2002, Song *et al.* 2003, Li and Rose 2001, Cawley *et al.* 2003).

Guided waves can propagate in different types of structures, such as bars, beams, plates and pipes. For two-dimensional (2D) waveguides, early studies were done by Rayleigh, Lamb, Stoneley and Love (Rose 1999). Guided waves have many advantages over other non-destructive evaluation techniques, such as cost effectiveness, large area monitoring, high sensitivity to small damage, suitable for in-situ monitoring and applicable to inaccessible area inspection. Since these techniques can be applied for in-situ monitoring of the structures, structural maintenance can be performed without any interruption in operation. Therefore, there is an increasing interest in utilizing guided waves for damage detection.

The majority of studies on guided waves have been carried out after 1990. Alleyne and Cawley (1991) implemented a 2D Fourier transform to study multimode propagating signals. This technique was used for measuring the contents of a signal in temporal and spatial frequency domain. It was shown that the 2D Fourier transform is an efficient technique when multiple wave modes cannot be separated in time domain due to geometrical conditions. Several mathematical models were proposed by Farmer *et al*. (1993) for a notched circular rod. Staudenmann (1995) assessed the feasibility of using guided waves for non-destructive testing. Zhu *et al*. (1998) investigated the feasibility of using guided waves for detecting corrosion. It was shown that higher frequency guided waves are more efficient for detecting surface defects. Fromme (2013) carried out a scattering analysis of guided waves. The study focused on fatigue and corrosion cracks in aircraft. It investigated the underlying problem of wave scattering at a circular through hole containing an arbitrarily orientated notch for the A_0 guided wave. The results showed that guided waves could be used to accurately detect the damages.

Lowe and Diligent (2002) carried out a finite element and experimental study on using fundamental symmetric mode (S_0) of guided wave for detecting damages in steel plates. In their study, reflection of guided waves from damages was investigated. Diligent et al. (2002) studied the feasibility of using S_0 guided wave for detecting circular damages in steel plates. The scattering problem of S_0 guided wave in a plate with a circular partly through thickness hole was studied and mode conversion of the guided waves was evaluated by finite element, analytical and experimental approaches. Guo and Cawley (2003) studied the interaction of guided waves with delaminations in a composite laminate. In their study, S_0 guided wave was used and delaminations were located at different interfaces. It was shown that the incident wave interacts with the delamination. Moreover, no wave reflection was observed if the delamination is located at the through-thickness locations with no shear stress.

Benmeddour *et al.* (2008) carried out a study on interaction of S_0 and A_0 guided waves at notches in aluminium plates. The results showed that S_0 guided waves are not sensitive to damages in some cases and finite element approach can predict the interaction of S_0 and A_0 guided waves scattered from the notches. Hayashi *et al.* (2005) employed a semi-analytical finite element

method to study the multiple reflections of S_0 and A_0 guided wave at delaminations in composite laminates. The results showed that the incident wave splits into two wave packets at the delamination with different arrival times and velocities. Moreover, multiple reflections were observed in their study. It was concluded that A_0 guided wave interacts with the delamination when it is located at different through-thickness locations, while S_0 guided wave may not interact with the delamination in some cases (e.g., when the delamination is located in the mid-plane of the composite laminate).

Veidt and Ng (2011) and Ng *et al.* (2012) carried out several studies on scattering of A_0 guided wave at through holes, delaminations and debondings at structural features in composite laminates. Numerical and experimental approaches were used in these researches. The results of the studies showed that the scattering characteristics of the guided waves in anisotropic materials could be very complicated. Moreover, delamination size to wavelength ratio and through-thickness location of the delaminations are two important factors, which affect the scattering characteristics of the guided wave. It was concluded that finite element approach could accurately predict the guided wave propagation in composite laminates. Ramadas *et al.* (2009) investigated the propagation of the A_0 guided wave in composite laminates consisting of a delamination through numerical and experimental approaches. It was shown that when A_0 guided wave interacts at the delamination, it converts from A_0 to S_0, which propagates in both sub-laminates at the delamination region as well as the laminate. It was concluded that mode conversion is expected when guided waves interact with the delamination.

Peng *et al.* (2009) investigated the interaction of guided waves with a delamination in an eight-ply composite laminate using 2D spectral element method. The interactions of S_0 and A_0 guided wave with the delamination were investigated. The results showed that A_0 guided wave is more robust for detecting delamination in composite laminates, especially when the delamination is at the mid-plane of the composite laminate. Zhou *et al*. (2008) studied the reflection and transmission of flexural modes in an isotropic beam with a crack through analytical approach. It was shown that the amplitudes of reflection and transmission coefficients depend on both the excitation frequency and location of the crack in the beam. Demčenko *et al*. (2006) numerically and experimentally studied the interaction of A_0 guided wave with a delamination in a composite laminate. It was concluded that additional A_0 modes would be generated due to mode conversion. Karthikeyan *et al.* (2009) investigated the interaction of A_0 guided wave with symmetric delaminations through numerical and experimental approaches. It was shown that S_0 guided wave would be generated due to mode conversion when the A_0 guided wave interacts with the delamination. Moreover, the generated S_0 guided wave only travels in the sub-laminates within the delamination region.

The present study focuses on scattering and mode conversion analysis of guided waves at delaminations in laminated composite beams. Additional wave component generated due to the interaction of incident wave with beam boundaries in the numerical simulations, which incur stretching effect on the beam, is investigated in this study. The scattering characteristics and mode conversion effect of guided waves at the delamination are then investigated in detail.

The organisation of this paper is as follows. Sec. 2 provides background information on guided waves and mode conversion phenomena. Sec. 3 describes the details of the 3D finite element simulation of the laminated composite beam. In Sec. 4, experiment setup is described and the finite element simulation results are verified by data measured using 3D scanning laser vibrometer. In Sec. 5, propagation characteristics of A_0 guided wave in the intact laminated composite beam are investigated and the phenomena of the new wave packets generation and stretching effect are also

discussed. The aim of this section is to investigate the generation of additional wave packets due to interaction of incident wave with the boundaries at the both sides of the beam cross-section. The propagation of guided wave in several laminated composite beams with a delamination is studied in Sec. 6. In this section, mode conversion due to the interaction of guided waves with the delamination is investigated, and the reflection and transmission coefficients are calculated and discussed in detail. Finally, conclusions are drawn in Sec. 7.

2. Guided waves and mode conversion phenomena

Elastic waves are mechanical waves that propagate in an elastic medium as an effect of forces associated with volume deformation and shape deformation of medium elements. Depending on restrictions imposed on the elastic medium, wave propagation character may vary. Bulk waves are elastic waves that propagate in infinite media and consist of two components; longitudinal waves and shear waves (Ostachowicz *et al.* 2012).

Guided waves are generated due to superposition of multiple reflections of longitudinal waves and shear waves. Guided wave is a general term that refers to elastic waves whose propagation characteristics depends on structural boundaries (Ostachowicz *et al.* 2012). Depending on boundary condition applied on media, three types of guided waves are expected. Rayleigh waves are surface guided waves that travel near the surface of the media (Rose 1999). Rayleigh waves include both longitudinal and transverse motions. Love waves (Rose 1999) propagate in 3D solids when a surface is bounded. Love waves are horizontally polarized surface waves and are characterised by particles oscillation in alternating transverse movement. Similar to Rayleigh waves, the particle motion amplitude decreases with depth of the 3D solids. Lamb waves were discovered by the famous British mathematician Horace Lamb who developed the theory of propagation of Lamb waves in solids in 1917. However, Lamb waves did not attract researchers due to complexity of understanding and generating of them. A comprehensive solution to Lamb waves was completed by Mindlin in 1950, followed by considerable details provided by Gazis in 1958. Lamb waves were not generated physically until 1961 when Worlton managed to generate and used them in damage detection. Later Fredrick and Worlton carried out experiments on Lamb waves (Ostachowicz *et al*. 2012) and Viktorov (1965) first evaluated the dispersive properties of Lamb waves.

Lamb waves are mechanical waves which propagate in infinite media bounded by two surfaces and are generated as a result of superstition of multiple reflections of longitudinal P waves and shear SV waves (Rose 1999). When Lamb waves propagate in structures, medium particle oscillation becomes very complex. Lamb waves are dispersive that means the value of wave velocity is dependent on the value of wave frequency (Ostachowicz *et al*. 2012). Three forms of Lamb wave propagate in a media depending on the distribution of stress and forces on the top and bottom surfaces; 1) symmetric modes (S_0, S_1, S_2,…), 2) anti-symmetric modes (A_0, A_1, A_2,…) and 3) shear horizontal modes (SH_0, SH_1, SH_2,…), of which symmetric and anti-symmetric modes have attracted researchers due to their efficiency in damage detection (Hayashi *et al*. 2005, Demčenko *et al.* 2006, Veidt *et al.* 2008, Ng *et al.* 2009, Veidt and Ng 2011, Ng and Veidt 2011, Ng *et al*. 2012). The number of Lamb wave modes is infinite contrary to bulk waves. Lamb waves would scatter and new wave modes could be generated when they encounter any discontinuity in their propagation path. Therefore, for implementing any Lamb wave based damage detection strategy, it is necessary to understand the interaction of Lamb waves with defects and

discontinuities in the structures

Kazys *et al*. (2006) investigated the interaction of S_0 guided wave with defects in steel plates through numerical approaches. It was shown that when S_0 guided wave interacts with defects, A_0 guided wave mode would be generated due to mode conversion effect. Ramadas *et al*. (2010) showed that when A_0 guided wave hits a delamination in a composite plate, mode conversions were observed due to the interaction between the incident wave and the delamination. The generated guided wave modes would undergo reflection and transmission at the delamination. The transmitted guided wave would propagate independently in the sub-laminates. It was observed that mode conversions resulted in reflections and transmission of both A_0 and S_0 modes. Moreover, turning modes (the modes that are generated from one side of the delamination to the other side, due to mode conversion at the ends of the delamination) and mode-converted turning modes would propagate from one sub-laminate to the other resulting in generation of numerous guided wave modes at both sides of the delamination.

3. Guided waves propagation in laminated composite beams

3.1 Numerical simulation and material properties

In this study, a 3D explicit finite element method was used to simulate cross-ply laminated composite beams with stacking sequence of $[0/90/0/90]_S$. The total thickness of the beam is 1.6 mm, which consists of eight 0.2 mm thick laminae. The length of the composite beams is 400 mm which is large enough to avoid the guided wave reflections from the right beam end. ABAQUS (2007) was used to model the laminated composite beam. Each lamina was modelled using eight-noded 3D reduced integration solid brick elements (C3D8R) with hourglass control. Each of the nodes of this element has three degrees-of-freedom (DOFs). Since C3D8R element is a reduced integration element, a model with C3D8I elements was also used to model the guided wave propagation and the results were compared against the results of using C3D8R. C3D8I element has more number of DoFs in its integration point in order to overcome the hourglassing problem of the reduced integration elements but it is computationally more expensive. Therefore, the results of these two types of elements were compared to ensure the capability of C3D8R elements in predicting the guided wave propagation. The lamina was assumed to be a VTM264 unidirectional carbon/epoxy prepreg tape with 0.55 fibre volume fraction, 1538 kg/m^3 density and 0.2 mm thickness. The elastic properties of the lamina were calculated using micromechanics theory by Chamis (1989) and are listed in Table 1.

To ensure the numerical stability and simulate the damping effect of composite materials, a small stiffness proportional damping was considered in the finite element model. The A_0 guided wave was excited by applying out-of-plane displacements to a 6 mm x 12 mm rectangular region on the left end of the beams. Solid elements with square dimensions of 0.4×0.4 mm^2 were used in the beam models. The thickness of each solid element was 0.2 mm, which is the thickness of the lamina, and hence, each lamina was modelled by one layer of solid elements. The small mesh size (0.4 mm×0.4 mm×0.2 mm) ensures the accuracy of the simulations. Ng and Veidt (2011) showed that the aspect ratio of the element equal to 2 is capable for simulating the propagation and scattering of the guided waves at delaminations in composite laminates.

Table 1 Elastic properties of the VTM264 prepreg lamina

E_{11} (GPa)	E_{22} (GPa)	E_{33} (GPa)	G_{12} (GPa)	G_{13} (GPa)	G_{23} (GPa)	$\boldsymbol{v_{12}}$	$\boldsymbol{v_{13}}$	$\boldsymbol{v_{23}}$
120.24	7.47	7.47	3.94	3.94	2.31	0.32	0.32	0.33

The dynamic simulation was solved using the explicit FE code in ABAQUS, which uses the central-difference integration. In this scheme, the integration operator matrix is inverted and a set of nonlinear equilibrium equations is solved at each time increment. Since the central different integration scheme is conditionally stable, the increment time step has to be small enough to ensure the stability. Stewart *et al.* (2006) recommended limiting the hourglass energy to less than 2% of the total energy to ensure the accuracy of predicting the guided wave propagation in solids. Bathe (1982) recommended the following condition in order to ensure the stability of the explicit analysis

$$\Delta t \leq \frac{L_{min}}{c_L} \tag{1}$$

where Δt is the time increment, L_{min} is the smallest mesh size and c_L is the longitudinal wave speed. In this study the time increment is automatically determined by ABAQUS for all simulations. Alleyne and Cawley (1991) recommended the following equation for determining the maximum mesh size in simulating the propagation of guided wave

$$l_e \leq \frac{\lambda_{min}}{10} \tag{2}$$

where l_e is the maximum mesh size and λ_{min} is the minimum wavelength size in the simulations.

3.2 Phase velocity calculation

The phase velocity of the guided waves c_p can be calculated by (Castaings and Hosten 2001)

$$c_p = \lambda f \tag{3}$$

where λ is wavelength and f is the central frequency of the propagating wave. Wavelength can be expressed in terms of wave number k as below

$$\lambda = \frac{2\pi}{k} \tag{4}$$

Wavenumber k is the rate of phase change in a certain distance and can be calculated as below

$$k = \frac{\Delta\phi}{\Delta x} \tag{5}$$

where $\Delta\phi$ is the phase change corresponding to measurement points with distance of Δx. Substituting wavenumber Eq. (5) into Eqs. (3) and (4) yields the following equation

$$c_p = \frac{2\pi f}{k} = \frac{2\pi f\ \Delta\phi}{\Delta x} \tag{6}$$

Hence, the phase velocity of the wave can be calculated using Eq. (6), in which the rate of phase change corresponding to two measurement points with distance of less than a wavelength.

3.3 Group velocity calculation

The group velocity is calculated from the energy density spectrum of the guided wave signals. The energy density spectrum can be calculated by continuous wavelet transform (CWT) (Veidt and Ng 2011).

$$WT(p,q) = \int_{-\infty}^{\infty} u(t)\chi_{p,q}^{*}(t)dt \tag{7}$$

where

$$\chi_{p,q}(t) = \frac{1}{\sqrt{q}}\,\chi\left(\frac{t-p}{q}\right) \tag{8}$$

p and q are wavelet transform factors. $u(t)$ is the out-of-plane displacement of the guided wave signal. The asterisk donates the complex conjugate. $\chi(t)$ is the mother wavelet which is Gabor wavelet and is defined as

$$\chi(t) = \frac{1}{\sqrt[4]{\pi}}\sqrt{\frac{\omega_0}{\eta}}\exp\left[-\frac{\left(\frac{\omega_0}{\eta}\right)^2}{2}\,t^2 + i\omega_0 t\right] \tag{9}$$

The time-frequency analysis resolution is affected by the value of ω_0 and η. These values are usually considered as $\omega_0 = 2\pi$ and $\eta = \pi\sqrt{2/ln2} \approx 5.336$. The energy density spectrum was calculated by $|WT(p,q)|^2$, which indicates the energy distribution of the signal around $t = p$, $\omega = \omega_0/q$ and was used to calculate the arrival time of the guided waves. The group velocity is defined as

$$c_g(f_c) = \frac{\Delta x}{\Delta t} \tag{10}$$

where Δt is the difference of the wave packet arrival times between two measurement points.

4. Verification of finite element models

4.1 Element type verification

The aims of this section are to verify the element type used in the finite element models. The model was the same eight-ply fibre reinforced composite beam as described in Sec. 3. Stacking sequence and material properties were the same as the laminated composite beam described in Sec.

3.1. The dimension of the composite beam was 400 mm x 12 mm x 1.6 mm. As discussed in Sec. 3.1, C3D8R elements were used in simulating the guided wave propagation. C3D8R and C3D8I elements were used to simulate the same laminated composite beams and the results were compared to investigate the accuracy of C3D8R elements in simulating the A_0 guided waves propagation. Fig. 1 shows the comparison between the results of the models using C3D8R and C3D8I elements. The excitation signal frequency was 140 kHz 6-cycle sinusoidal tone burst pulse modulated by Hanning window and the measurement point was located at 50 mm from the left beam end (the excitation location). As shown in Fig. 1 there is a very good agreement between the results of two models. Therefore, C3D8R element was used for the rest of the studies in this paper.

4.2 Experimental verification of FE models

This section presents a study of the A_0 guided wave propagation in the $[0/90/0/90]_S$ fibre reinforced composite beam. The finite element model described in Sec. 3.1 was validated by means of phase and group velocity of the guided waves in this section. The measured data of four measurement points with 4 mm distance away from each other was used to calculate the group and phase wave velocity. The simulation results are compared with the experimental results to ensure that the finite element simulations are able to accurately predict the propagation of guided waves in the composite beams.

The experimental data was obtained using Polytec Scanning Vibrometry (PSV-400-3D-M), which could be used for scanning 3D vibration and geometric data. A $[0/90/0/90]_S$ intact composite beam was manufactured using eight layers of unidirectional carbon/epoxy prepreg lamina with the material properties shown in Table 1. The material properties of the lamina were the same as the lamina used in the FE simulations. The length of the composite beam was 285 mm with 12 mm×1.6 mm cross-section. A 12 mm×6 mm×2 mm rectangular piezoceramic was adhesively bonded to the composite beam end to excite the A_0 guided wave. A backing mass with 2 mm thickness was adhesively bonded to the piezoceramic transducer to maximise the excitability of the A_0 guided wave.

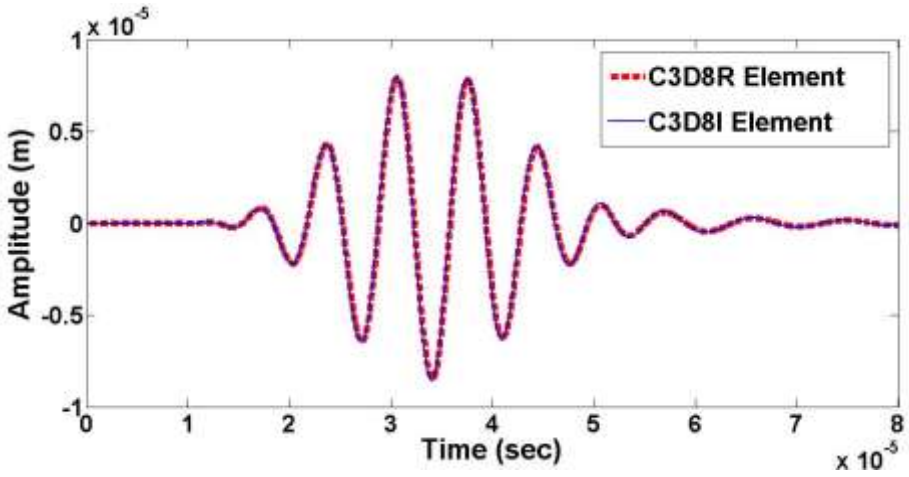

Fig. 1 Comparison between the simulations results using C3D8R and C3D8I

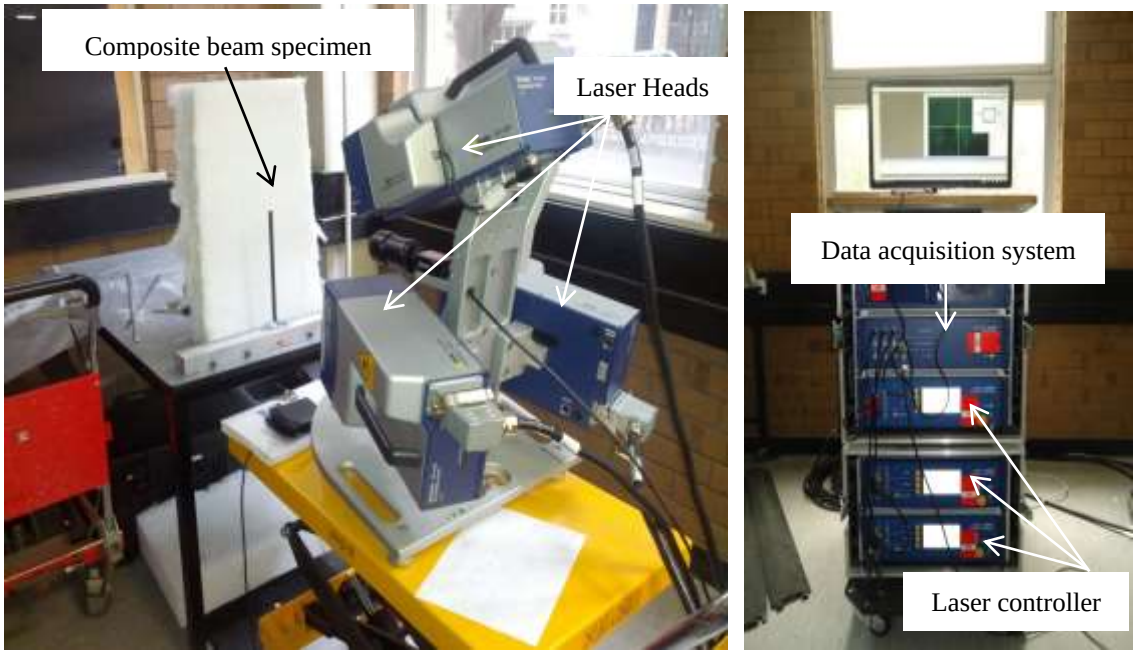

Fig. 2 Experiment setup

The excitation signal was generated by a computer controlled signal generator with 10 V peak-to-peak output voltage. An amplifier was used to amplify the excitation signal by a factor of 5. The out-of-plane displacements were measured by the laser heads and the data was sent to the laser controller and data acquisition system for post-processing. To improve the signal-to-noise ratio, a band-pass filter was introduced to the system and the average of signals was calculated over 5000 acquisitions. Fig. 2 shows the experiment setup used in this study.

The study considered a 5-cycle sinusoidal tone burst pulse modulated by Hanning window. The excitation frequency is from 20 kHz to 300 kHz with steps of 20 kHz. The signal was measured at four consecutive measurement points with 4 mm away from each other. The group velocity is calculated by dividing the distance between measurement points (4 mm) over the difference of the arrival times of the signals at each pair of measurement points (Eq. (10)). Similarly, the phase velocity is obtained by calculating the phase change of the signals between a pair of measurement points and then substitutes it into Eq. (6). The phase and group velocity of the wave at each excitation frequency was calculated by averaging the calculated velocities from these four measurement points. Figs. 3 and 4 show the phase and group velocity dispersion curves calculated using the data from finite element simulations and experiments.

Fig. 5 shows the signal output obtained from the finite element simulation and experiment for a measurement point located at 50mm from the left beam end (the excitation location). In this case, the excitation signal frequency was 120 kHz. At this frequency, the phase and group velocities obtained from FE are 1122 m/s and 1400 m/s, respectively, and the corresponding values obtained

from experiment are 1202 m/s and 1453 m/s, which are in good agreement. However, the time domain results shown in Fig. 5 show that there is a small phase shift between the results obtained from finite element simulation and experiment. It was confirmed that the small phase shift was caused by a small difference between the location of measurement points in the finite element and experiment due to human error. The time difference between two wave packets is 0.4 μs, which equals 0.6 mm measurement location error. However, as can be seen from Figs. 3 and 4, the phase and group dispersion curves calculated from both approaches show a good agreement. Therefore, the finite element simulations are able to predict the propagation of guided waves in fibre reinforced composite beams.

5. Guided wave propagation in an intact composite beam

The aim of this section is to investigate the A_0 guided wave generation and propagation in an intact composite beam. The length of the beam is 1000 mm with 12 mm×1.6 mm cross-section, and material properties of the lamina, stacking sequence and number of layers are the same as the model used in Sec. 3.1. The length of model was considered long enough (400 mm) to avoid any wave reflection from the beam ends.

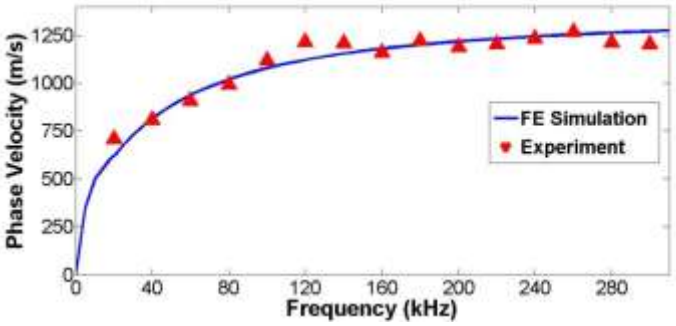

Fig. 3 Comparison between phase velocity dispersion curve obtained from FE simulation and experiment

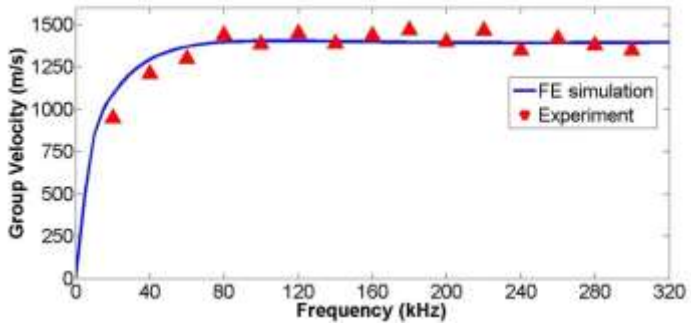

Fig. 4 Comparison between group velocity dispersion curve obtained from FE simulation and experiment

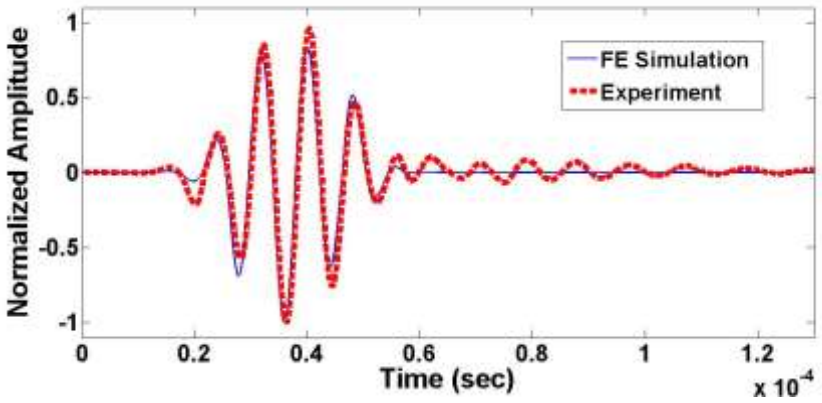

Fig. 5 Comparison of the signal obtained from FE simulation and experiment (excitation frequency is 120 kHz)

The guided wave was measured at nine consecutive points (Points a to i) with equal distance of 50mm away from each other, and the first measurement point (Point a) was at 50 mm from the excitation location. The excitation signal was a 5-cycle sinusoidal tone burst pulse modulated by Hanning window with central frequency at 120 kHz. Fig. 6 shows the finite element simulation of the incident A_0 guided wave propagation in the beam. The time-displacement histories in Z and Y direction for nine measurement points (Points a to i) are shown in Figs. 7(a) to 7(i).

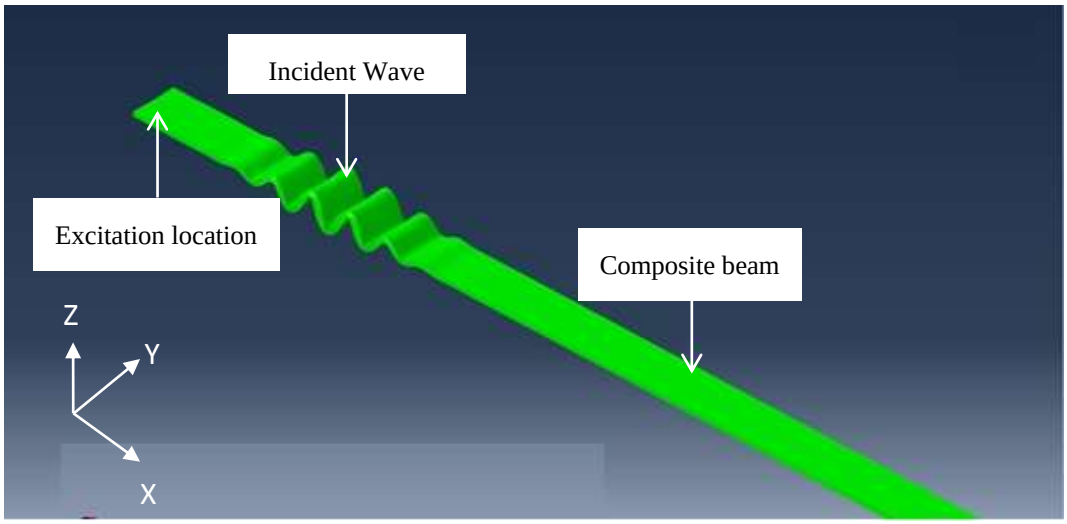

Fig. 6 Propagation of incident A_0 guided wave in an intact composite beam – Scale factor = 1000

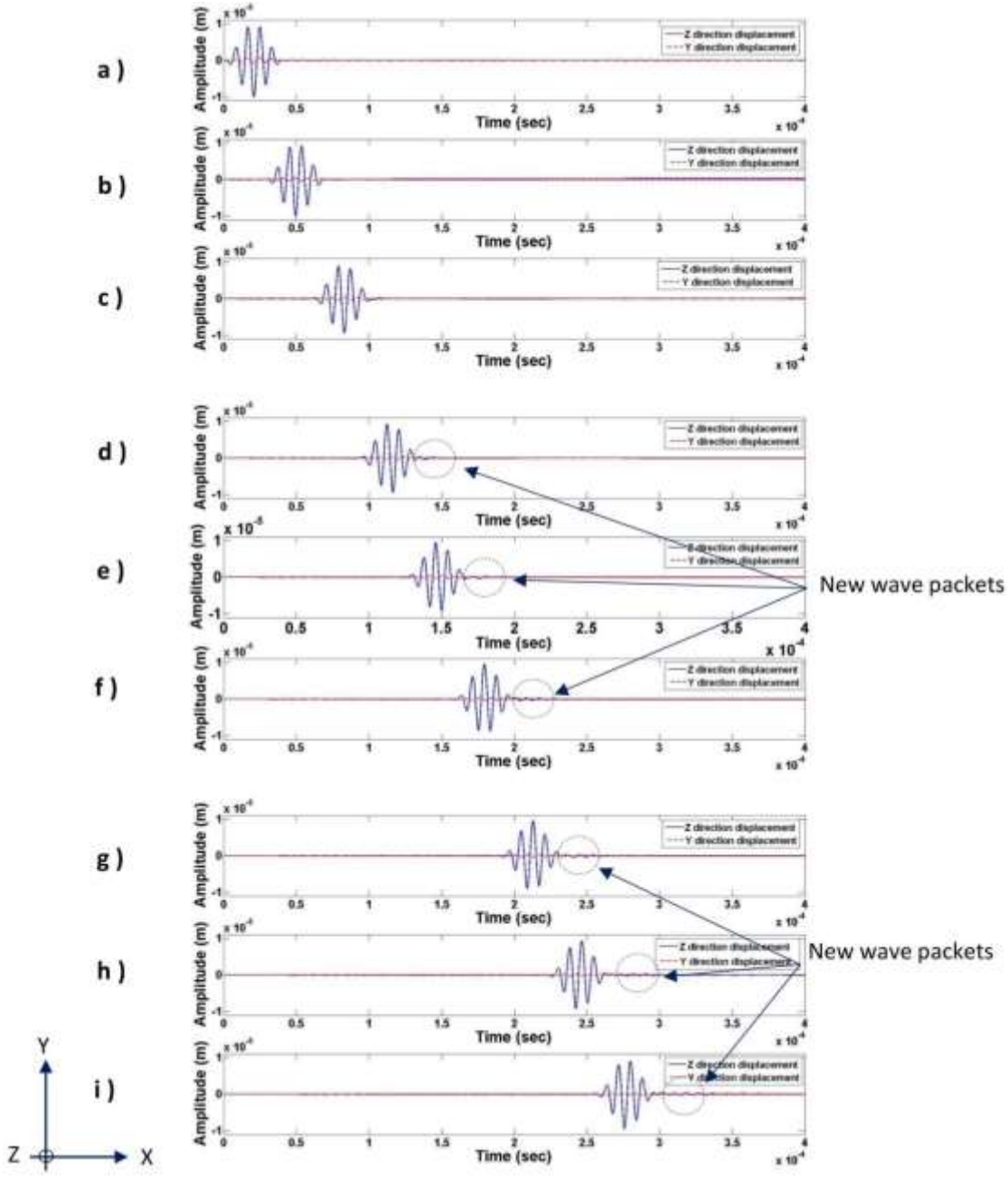

Fig. 7 Z and Y direction displacements at the measurement points – Intact composite beam – $[0/90/0/90]_S$ – Excitation frequency = 120 kHz (Points a to i, 50 mm – 400 mm from the excitation location)

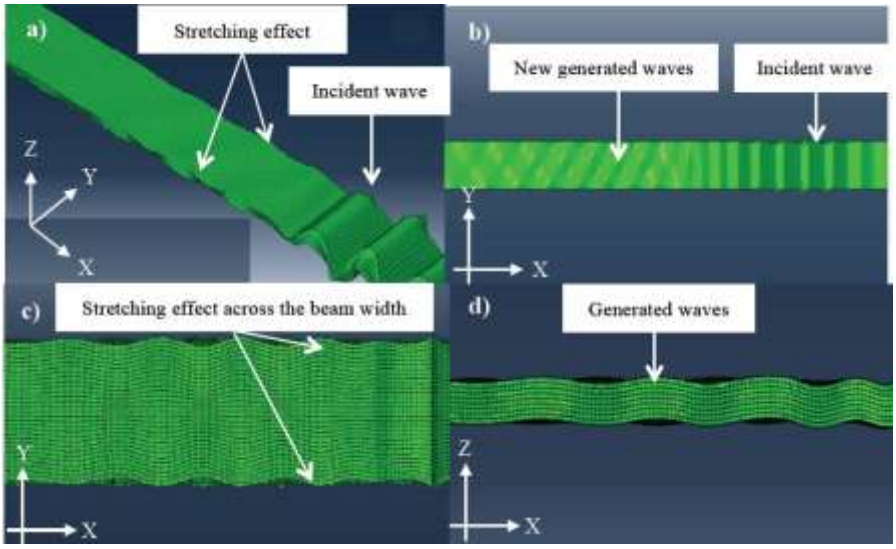

Fig. 8 (a) 3D deformation of the beam due to stretching effect, (b) deformation of the beam due to propagation of incident and generated waves, (c) deformation of the beam in Y direction due to stretching effect, and (d) deformation of the beam in Z direction due to generated waves – Scale factor = 1000

The group velocity calculated using finite element simulation data was 1400 m/s. As shown in Figs. 7(a) to 7(c), Z direction displacement of the incident wave has no extra components. However, as the incident wave travels, new wave packets exist in the signal. Figs. 7(g) to 7(i) show that a couple of wave packets are traveling with the incident wave and then completely separate from the incident wave. The observation of the finite element simulation results show that these new wave packets are generated when the incident A_0 guided wave interacts with boundaries at the both sides of the beam cross-section. The group velocity of these wave packets is 1395 m/s, which was calculated at some measurement points, where the new wave packets separate from the incident wave signal. The velocity of these wave packets is very close to the group velocity of the incident A_0 guided wave.

Moreover, Y direction displacement plots in Fig. 7(a) to 7(i) show that in addition to the main signal several wave packets travel behind the incident wave with a small time delay. Similar to the main signal, these wave packets impose Y direction particle motion on the beam. The snapshots from finite element simulation output show that the main signal and these waves have stretching effects on the beam, which is symmetric across the beam. Therefore, this effect is referred as stretching effect in this paper. The group velocity of stretching effect in Y direction was calculated as 1400 m/s for the main signal and 1395 m/s for new wave packets, which is equal to group velocity of the incident wave and new wave packets calculated in Z direction. The plots show that each travelling wave packet including incident wave and new generated wave packets impose stretching effects on the beam. However, incident wave possessed the largest stretching effect amplitude. Figs. 8(a) to 8(d) show the 3D deformation of the beam due to stretching effect, deformation of the beam due to generated waves and incident wave, deformation of the beam across the beam width in Y direction, and displacement of the beam in Z direction due to stretching effect, respectively.

As discussed, the finite element results show that the new wave packets are generated as incident wave travels throughout the beam, which mainly cause particle motion in Z direction (Figs. 7(d) to 7(i) and Figs. 8(b) and 8(d)). Moreover, the signal outputs and snapshots show that each wave packet including incident wave and generated wave packets impose stretching effects in the beam which causes particle motion in Y direction (Fig. 8(a)) as well. Z direction particle motion is similar to that of anti-symmetric mode but stretching effect cause symmetric displacement in Y direction which has zero value in the beam mid-plane as shown in Figs. 8(b) and 8(c). Since the incident wave signal and generated wave packets interact with beam boundaries throughout the beam, this phenomenon happens infinitely and imposes stretching effects with smaller amplitudes than the incident wave. It should be noted that these two unique phenomena (generation of new wave packets and stretching effect) have not been observed and reported previously in plates.

6. Mode conversion and scattering analysis of guided waves in delaminated composite beams

6.1 Numerical case studies

Several finite element models were considered in this section. The length of the beams was 400 and the cross-section was 12mm×1.6mm. Each composite beam contains eight plies. The material properties of the lamina and stacking sequence of the beams have been described in Sec. 3.1. The delaminations were across the full width of the beams and it was assumed that the delaminations were located at the centre of the beam as shown in Fig. 9. The wavelength of the A_0 guided wave calculated by DISPERSE (2003) is 8.0mm at 140 kHz, which was used to calculate the delamination size (d) to wavelength (λ) ratio as shown in Table 2. Delaminations located at different through-thickness locations were considered in this study and all damage cases are summarised in Table 3. There are two measurement points, Points A and B, as shown in Fig. 9, which were 150 mm away from the beam ends, respectively. At each of these measurement points, both in-plane and out-of-plane displacements were calculated at the top and bottom surfaces of the beam. The data was then used to investigate the characteristics of the guided wave reflected and transmitted at the delaminations.

Table 2 Delamination size to wavelength ratios for all damage cases

Damage case	d/λ= 0.5	d/λ= 0.75	d/λ= 1.00	d/λ= 2.00
Delamination size (mm)	4	6	8	16

Table 3 Damage case studies for delamination at different through-thickness locations

Damage case	1	2	3	4
Delamination through-thickness location	Between 1st & 2nd layer	Between 2nd & 3rd layer	Between 3rd & 4th layer	Between 4th & 5th layer

The distance between the excitation point and the first measurement point was more than the four wavelengths that fulfils the far-field wave field solution requirement (Moreau and Castaings 2008). The delaminations were modelled by separating the finite element nodes at the delamination region, which allows two interfaces at the delaminated region move independently. No contact interaction was considered in the finite element models, which allows the interpenetration of sub-laminates at the delamination region. Fig. 9 shows a schematic diagram of the set up used in the finite element simulations for the beam models with a delamination located at the centre of the beam. The A_0 guided wave was excited by applying out-of-plane displacements to a rectangular region at the left beam end. However, it should be noted that generation of S_0 guided wave mode with small amplitude was inevitable due to Poisson effect. The excitation signal is a 5-cycle narrow-band sinusoidal tone burst pulse modulated by Hanning window with central frequency of 140 kHz. Figs. 10(a) to 10(c) show the excitation signal in time domain, frequency domain (fast Fourier transform) and time and frequency domain (continuous wavelet transform), respectively.

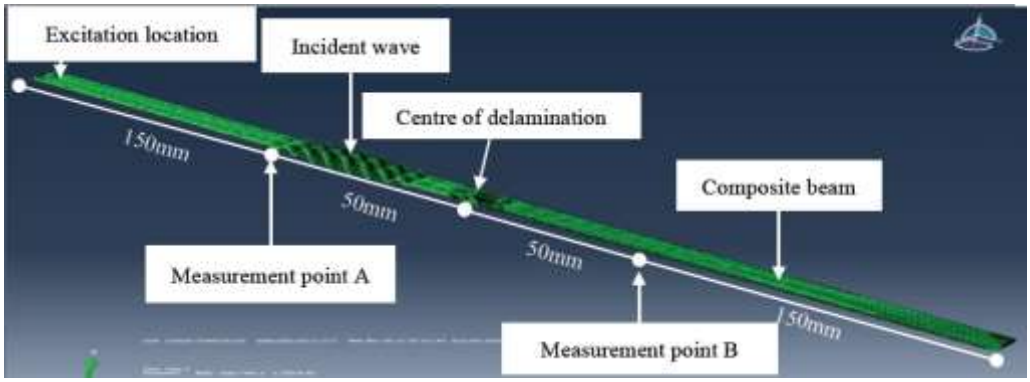

Fig. 9 Schematic diagram of FE simulation setup for beam with a delamination - Scale factor = 500

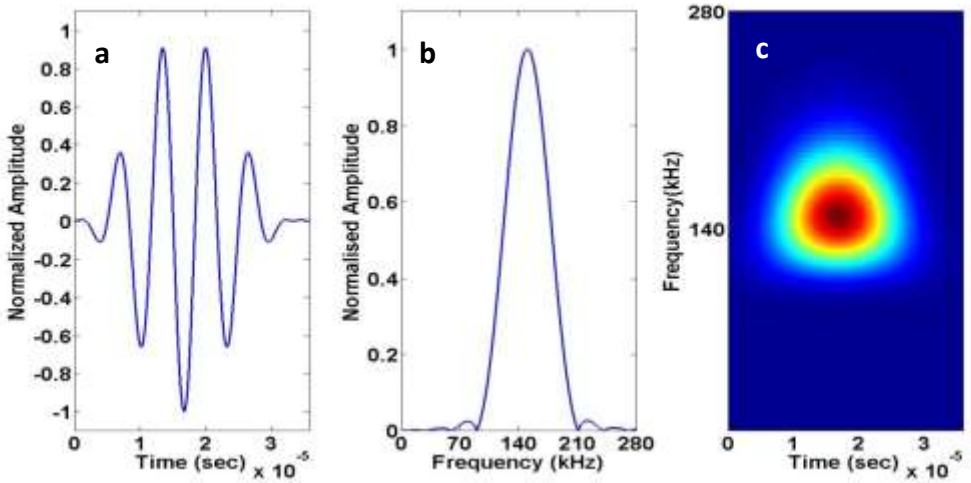

Fig. 10 Excitation signal in (a) time domain (b) frequency domain (c) time-frequency domain

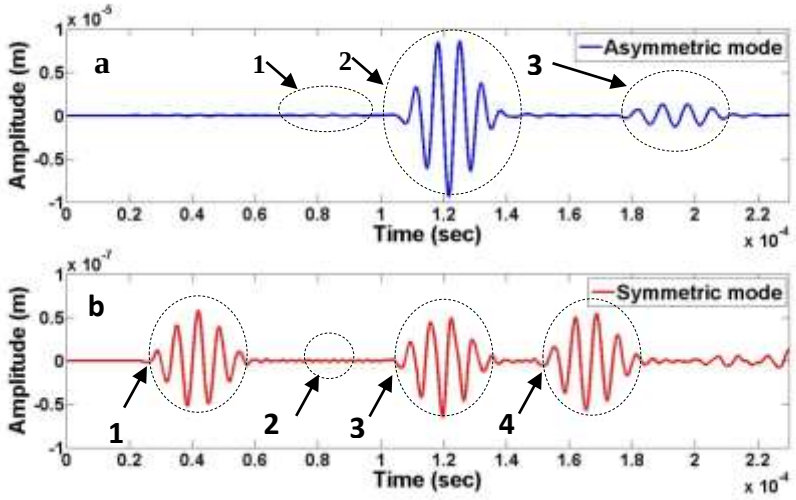

Fig. 11 Out-of-plane displacement at measurement Point A– Damage case 3 - d/λ= 0.5 (a) A_0 and (b) S_0 guided wave

6.2 Mode conversion analysis

When guided waves are generated, the symmetric wave modes mainly cause in plane particle motion while the dominant direction of particle displacement for anti-symmetric wave modes is out-of-plane (Rose 1999). For the fundamental guided wave modes, A_0 mode has anti-symmetric out-of-plane displacement and symmetric in-plane displacement, and S_0 mode has symmetric out-of-plane displacement and anti-symmetric in-plane displacement. In the finite element models, the time history of out-of-plane displacement at the measurement points was extracted. The out-of-plane displacement of pure anti-symmetric mode of guided waves can be extracted by adding the out-of-plane displacements at the top and bottom surfaces of the beam. The out-of-plane displacement of pure symmetric guided waves can be extracted by subtracting the out-of-plane displacement of pure anti-symmetric mode of guided waves from the out-of-plane displacement at top or bottom surfaces of the beam. It should be noted that since the amplitudes of the extracted wave signals are doubled due to the summation and subtraction of the measurements at the top and bottom surfaces of the beam, the amplitudes needs to divide by two before they are used in studying the mode conversion effects and scattering characteristics. The mode conversion effects of the A_0 guided wave at delaminations with different sizes and through-thickness locations were investigated and all damage cases are summarised in Tables 2 and 3.

Figs. 11(a) and 11(b) show the out-of-plane displacement at measurement Point A and Figs. 12(a) to 12(i) shows the snapshots of displacement from 20μs to 300μs with time step of 20 μs for damage case 3 and d/λ= 0.5 The theoretical group velocity of A_0 and S_0 guided wave at frequency of 140 kHz was calculated as 1400m/s and 6450m/s, respectively, which are then used for

identifying each wave packet in the signal outputs. The group and phase velocity were calculated by finite element simulation using intact composite beams and then verified by experimentally measured data.

The arrival time of each wave packet was calculated by determining the wave envelope through Hilbert transform. As shown in Fig. 11(a), the arrival time of wave packet (1) at measurement Point A using signal output was calculated as 69.2 μs. Fig. 12(c) shows this wave packet is generated when S_0 wave arrives at the delamination. The time required for S_0 wave to arrive at the delamination is 31.0 μs and S_0 to A_0 converted wave packet ($S_0 - A_0$) takes 35.7 μs to return to measurement Point A. Hence, the total travel time of S_0 wave from excitation location to the delamination plus travel time of $S_0 - A_0$ wave packet to Point A is 66.7 μs, which agrees with arrival time of wave packet (1) from signal output. Therefore, this wave packet is referred as $S_0 - A_0$ mode converted wave packet due to interaction of S_0 wave with the delamination.

The arrival time of wave packet (2) at measurement Point A was calculated as 105.6 μs. The theoretical arrival time of incident wave at this measurement point is 107.1 μs, which agrees with finite element result. Similarly, the arrival time of third wave packet (3) in Fig. 11(a) was calculated as 176.3 μs. The theoretical arrival time of reflected A_0 wave from delamination was calculated as 178.5 μs, which agrees with FE result (Fig. 12(i)). Hence, the wave packet (2) is referred as A_0 incident wave and wave packet (3) is referred as reflected A_0 wave from delamination (R_{A0}).

Fig. 11(b) depicts the out-of-plane displacement caused by symmetric mode at measurement point A. Since the symmetric mode of guided wave has higher group velocity, it is expected to generate more reflections and transmissions in the same time window compared to anti-symmetric mode guided wave. The arrival time of the first wave packet (1) at measurement Point A using signal output (Fig. 11(b)) was calculated as 24.1 μs.

The theoretical arrival time of the incident wave at Point A is calculated as 23.3 μs, which agrees with finite element simulation results. Hence, this wave packet is referred as incident wave (Fig. 12(b)). The arrival time of second wave packet (2) obtained from signal output was calculated as 83.6 μs, which equals the required time for reflected wave from delamination and left end (RR_{S0}) to arrive at Point A calculated by dividing corresponding distance by theoretical S_0 wave group velocity (85.3 μs). This wave packet has smaller amplitude compared to the wave packet (1) because symmetric mode causes small reflection from delamination when delamination is located between third and fourth layer (Hayashi 2002). Therefore, wave packet (2) is defined as reflected S_0 wave from delamination and beam left end (RR_{S0}).

The arrival time of third wave packet (3) was calculated as 101.3 μs, which equals to the travel time of the transmitted S_0 wave reflect from the beam right end and arrive at measurement Point A (100.8 μs) (Fig. 12€), which is referred as RT_{S0}. The small wave packets between wave packets 2 and 3 are multiple reflections of wave packet (3) from left end and delamination, which can be seen in Fig. 12.

The wave packet (4) in Fig. 11(b) has an arrival time of 149.6.8 μs. The snapshot (Fig. 12(h)) shows that this wave is generated when incident A_0 guided wave arrives the delamination. Therefore the incident wave undergoes mode conversion and then mode converted wave packet ($A_0 - S_0$) propagates in the beam as S_0 guided wave. This agrees with theoretical travel time for A_0 guided wave traveling to the delamination (142.9 μs) plus the travel time of mode converted S_0 wave ($A_0 - S_0$) to research the measurement Point A (7.8 μs).

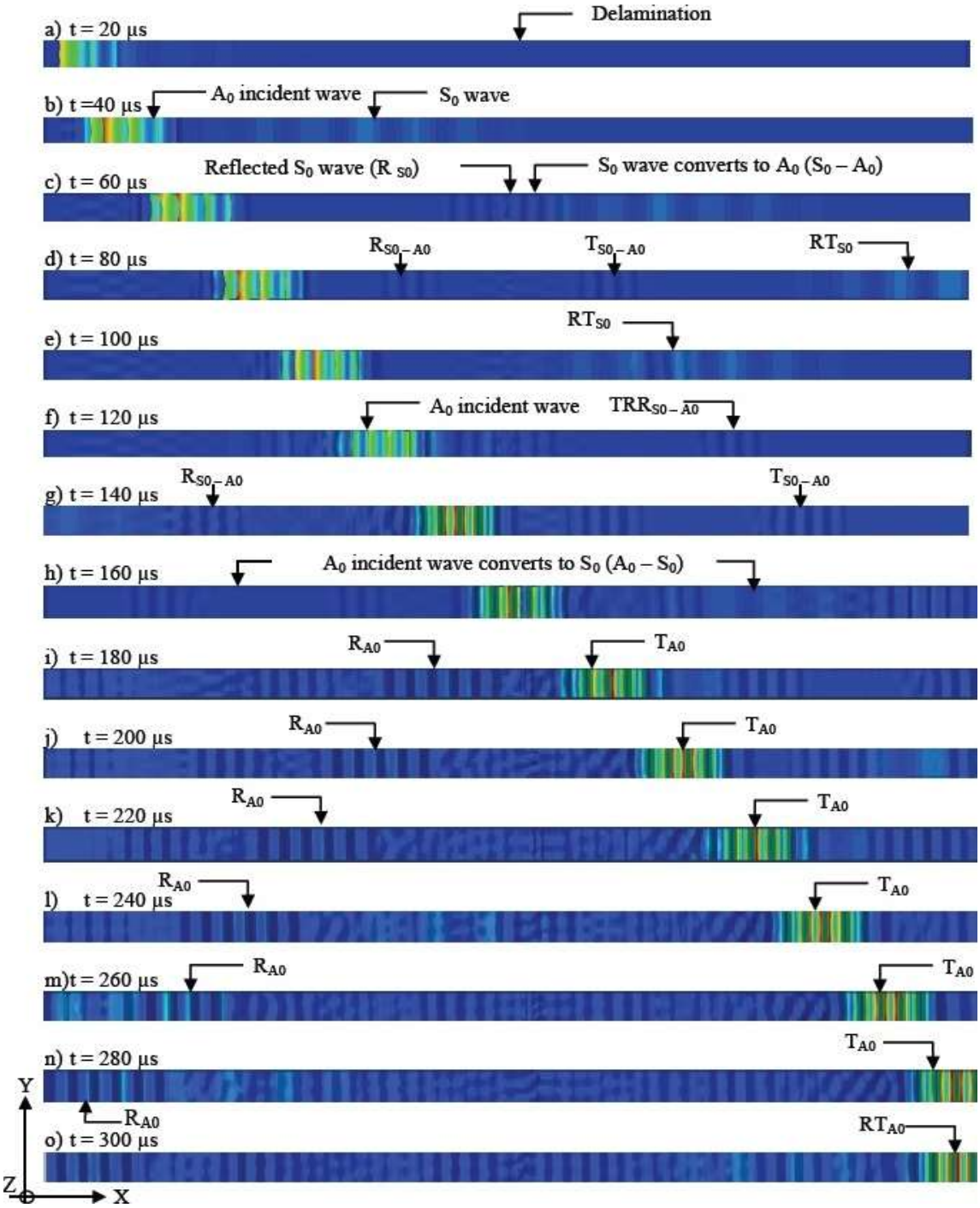

Fig. 12 Snapshots of displacement at 20 μs to 300 μs with time step of 20 μs - Damage case 3 - d/λ= 0.5

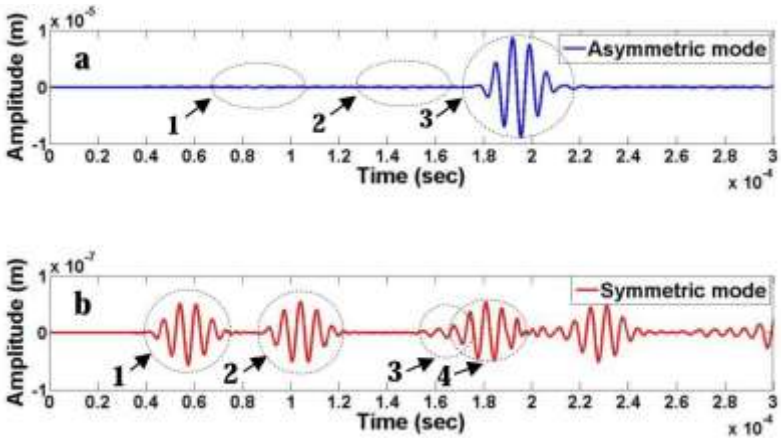

Fig. 13 Out-of-plane displacement at measurement Point B– Damage case 3 - d/λ= 0.5 (a) A_0 and (b) S_0 guided wave

Table 4 Captured A_0 guided waves at measurement Point B

Captured wave packet (Fig. 13(a))	Arrival time according to signal output (μs)	Theoretical arrival time (μs)	Wave packet
1	65.1	66.7	T_{S0-A0} (Fig. 12(d))
2	131.3	128.7	TRR_{S0-A0} (Fig. 12(f))
3	176.5	178.4	T_{A0} (Fig. 12(i))

Table 5 Captured S_0 guided waves at measurement Point B

Captured wave packet (Fig. 13(b))	Arrival time according to signal output (μs)	Theoretical arrival time (μs)	Wave packet
1	40.2	38.8	T_{S0}
2	88.9	85.3	RT_{S0} (Fig. 12(e))
3	152.1	150.5	T_{A0-S0} (Fig. 12(h))
4	158.0-163.0	162.7	RRT_{S0}

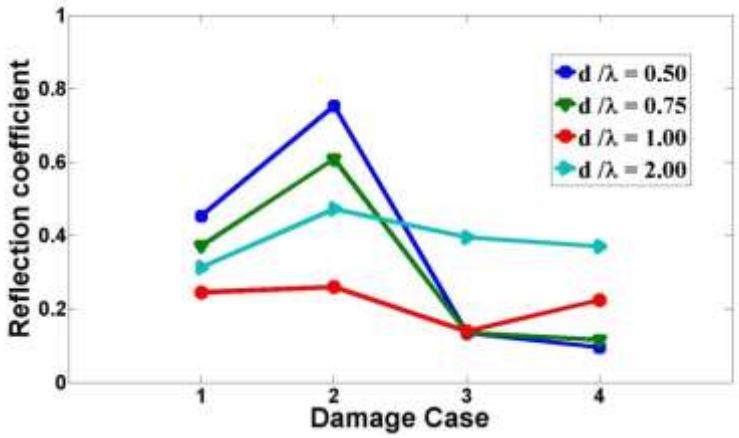

Fig. 14 Reflection coefficients for different case studies

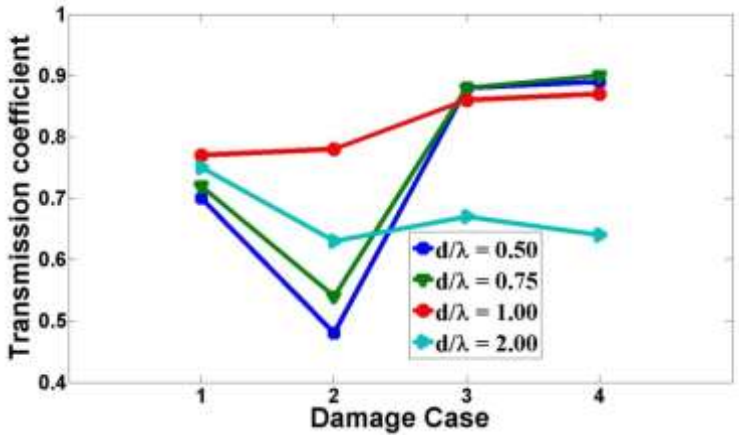

Fig. 15 Transmission coefficients for different case studies

Fig. 13 depicts the out-of-plane displacement for measurement Point B. The arrival time calculated from signal output, and theoretical arrival time according to the travel distance and group velocity have been summarized in Tables 4 and 5. As shown in Table 5, the mode converted wave packets have been captured in measurement Point B.

The results of this section can be summarized as follows: i) both A_0 and S_0 guided waves propagate in composite beam when A_0 guided wave is excited. ii) Since group velocity of S_0 guided wave is higher than A_0 guided wave, S_0 guided wave arrives at delamination first and undergoes mode conversion ($S_0 – A_0$). iii) In addition, S_0 guided wave is reflected and transmitted, and undergoes mode conversion again when it arrived at delamination after it reflected from the beam ends. iv) Generated $S_0 – A_0$ wave undergoes mode conversion when arrived at delamination ($S_0 – A_0 – S_0$). v) Incident A_0 guided wave undergoes mode conversion ($A_0 – S_0$) when it interacts

with the delamination. vi) Generated $A_0 - S_0$ wave is reflected from beam ends. vii) Reflected wave packet undergoes mode conversion ($A_0 - S_0 - A_0$) when arrived at delamination. Therefore, incident waves undergo multiple mode conversions due to interaction with the delamination. This applies for both A_0 and S_0 guided waves.

6.3 Reflection and transmission coefficients of scattered waves

In this section the reflection and transmission coefficients of guided waves were calculated in the damage case studies. The reflection coefficient is defined as the ratio of amplitude of reflected wave to the amplitude of incident wave at the centre of delamination. The transmitted coefficient is defined as the ratio of amplitude of transmitted wave to the amplitude of the incident wave measured at the centre of delamination.

Measurement Points C and D are located at 100mm and 300mm from the excitation point, respectively, and the out-of-plane displacement history for these two measurement points was recorded. The data at the measurement Points C and D was used for calculating the reflection and transmission coefficient, respectively.

Figs. 14 and 15 show the reflection and transmission coefficients for damage case with different delamination to the wavelength ratios as described in Sec 6.1. The results show that the maximum reflection and minimum transmission coefficient occur when the delamination is located between second and third layer (damage case 2). The minimum reflection and maximum transmission occur when delamination is located symmetrically in the middle of the beam (between fourth and fifth layer) (damage case 4).

7. Conclusions

This paper studied the A_0 guided wave propagation and scattering characteristics in fibre reinforced composite beams at the low frequency regime. The guided wave propagation and scattering characteristics at the delaminations in composite beams was studied using the 3D finite element simulations. Good agreement was found between finite element calculated and experimentally measured phase and group velocity.

Extended studies on scattering characteristics of A_0 guided wave in intact composite beams showed that several wave packets are generated due to interaction of guided wave with the boundaries at the both sides of the beam cross-section. The results showed that the incident wave and generated wave packets incur stretching effect, which propagate in the beam as well. This shows that interaction of incident wave with beam cross-section boundaries incur some unique phenomena that do not exist in plates and should be considered carefully during the data analysis.

The study also investigated the scattering characteristics of A_0 guided wave propagation in several delaminated composite beams with different delamination to wavelength ratios and different delamination through-thickness locations. Signal processing technique, Hilbert transform, was performed to extract the arrival time of waves reflected from the delaminations and beam ends. S_0 and A_0 guided waves were extracted by using the measured nodal displacement at the top and bottom surfaces of the beam. The results showed that when S_0 and A_0 guided waves interact with delamination, they undergo mode conversions. The results showed that S_0 guided waves convert to A_0 guided waves, and the mode converted A_0 guided waves convert to S_0 guided waves when they interacts with the delaminations.

The study was then extended to investigate the reflection and transmission coefficients of the guided wave at the delaminations. The results showed that maximum wave reflection occurs when delamination is located between second and third interfaces while maximum wave transmission occurs when delamination is located between fourth and fifth layers. The findings of this study can improve the performance for guided wave damage detection techniques.

Acknowledgements

This work was supported by the Australian Research Council under Grant Number DE130100261. The supports are greatly appreciated.

References

ABAQUS Theory Manual Version 6.7 (2007), ABAQUS Inc, Sunnyvale, CA 94085, USA.

Alleyne, D. and Cawley, P. (1991), "A two-dimensional Fourier transform method for the measurement propagating multimode signals", *J. Acoust. Soc. Am.*, **89**, 1159-1168.

Bathe, K J. (1982), *Finite Element Procedures in Engineering Analysis*, Prentice-Hall, Upper Saddle River, *New Jersey*, USA.

Benmeddour, F., Grondel, S., Assaad, J. and Moulin, E. (2008), "Study of the fundamental Lamb modes interaction with symmetrical notches", *NDT & E Int.*, **41**(1), 1-9.

Castaings, M. and Hosten, B. (2001), "Lamb and SH waves generated and detected by air-coupled ultrasonic transducers in composite material plates", *NDT & E Int.*, **34**(4), 249-258

Cawley, P., Lowe, M.J.S., Alleyne, D.N., Pavlakovic, B. and Wilcox, P. (2003), "Practical long range guided wave testing: Applications to pipes and rail", *Mater. Evaluation*, **61**, 66-74.

Chamis, C.C. (1989), "Mechanics of composite materials: Past, present and future", *J. Compos. Technol. Res.*, **11**, 3-14.

Demčenko, A., Žukauskas, E., Kažys, R. and Voleišis, A. (2006), "Interaction of the A0 Lamb wave mode with a delamination type defect in GLARE3-3/2 composite material", *Acta Acustica united with Acustica*, **92**(4), 540-548.

Diligent, O., Grahn, T., Boström, A., Cawley, P. and Lowe, M. (2002), "The low frequency reflection and scattering of the s0 Lamb mode from a circular through-thickness hole in a plate: Finite element, analytical and experimental studies", *J. Acoust. Soc. Am.*, **112**(6), 2589-2601.

Farmer, S.C., Sayir, A. and Dickerson, P.O. (1993), *In situ Composites*, Science and Technology, TMS, Warrendale, Pennsylvania, USA.

Fromme, P. (2013), "Health Monitoring of Structural and Biological Systems", *Proceedings of SPIE - The International Society for Optical Engineering*, *8695*, San Diego, April.

Guo, N. and Cawley, P. (1993), "The interaction of Lamb waves with delaminations in composite laminates", *J. Acoust. Soc. Am.*, **94**(4), 2240-2246.

Hayashi, T. and Kawashima, K. (2002), "Multiple reflections of lamb waves at a delamination", *Ultrasonics*, **40**(1-8),193-197.

Hayashi, T., Kawashima, K., Sun, Z. and Rose, J. (2005), "Guided wave propagation mechanics across a pipe elbow", *J. Press. Vessel Technol.*, **125**(3), 322-327.

Hongerholt, D.D., Willms, G. and Rose, J.L. (2002), "Summary of results from an ultrasonic in-flight wing ice detection system", *Review of Progress in Quantitative Nondestructive Evaluation*, **21**, 1023-1028.

Karthikeyan, P., Ramadas, C., Bhardwaj, M.C. and Balasubramaniam, K. (2009), "Non-contact ultrasound based guided Lamb waves for composite structure inspection: some interesting observations", *Proceedings of the AIP Conference Proceedings*, New York, March.

Kazys, R., Demcenko, A., Zukauskas, E. and Mazeika, L. (2006), "Air-coupled ultrasonic investigation of multi-layered composite materials", *Ultrasonics* ,**44**, 819-822.

Kovic, B. and Lowe, M. (2003), *DISPERSE User's Manual Version 2.0.16B,* Imperial College, University of London, Non-Destructive Testing Laboratory, London, United Kingdom.

Li, J. and Rose, J.L. (2001), "Guided wave testing of containment structures", *Mater. Evaluation*, **59**(6), 783-787.

Li, Z. and Wanchun, Y. (2008), "Power reflection and transmission in beam structures containing a semi-infinite crack", *Acta Mechanica Solida Sinica*, **21**(2), 177-188.

Lowe, M.J.S. and Diligent, O. (2002), "The low frequency reflection characteristics of the fundamental symmetric Lamb wave S0 from a rectangular notch in a plate", *J. Acoust. Soc. Am.*, **111**, 64-74.

M. Staudenmann. (1995), "Structural waves in non-destructive testing", Ph.D Dissertation, ETH Zürich, Zürich.

Moreau, L. and Castaings, M. (2008), "The use of an orthogonality relation for reducing the size of finite element models for 3D guided waves scattering problems", *Ultrasonics*, **48**(5), 357-366.

Ng, C.T. (2014a), "Bayesian model updating approach for experimental identification of damage in beams using guided waves", *J. Struct. Health Monit.*, **13**(4), 359-373.

Ng, C.T. (2014b), "On the selection of advanced signal processing techniques for guided wave identification using a statistical approach", *J. Eng. Struct.*, **67**, 50-60.

Ng, C.T. (2015), "A two-stage approach for quantitative damage imaging in metallic plates using Lamb waves", *Earthq. Struct."*, **8**(4), 821-841.

Ng, C.T., Veidt, M. and Rajic, N. (2009), "Integrated piezoceramic transducers for imaging damage in composite laminates", *Proceedings of SPIE*, Weihai, October

Ng, C.T. and Veidt, M. (2011), "Scattering of the fundamental anti-symmetric Lamb wave at delaminations in composite laminates", *J. Acoust. Soc. Am.*, **129**(3), 1288-1296.

Ng, C.T., Veidt, M., Rose, L.R.F. and Wang, C.H. (2012), "Analytical and finite element prediction of Lamb wave scattering at delaminations in quasi-isotropic composite laminates", *J. Sound Vib.*, **331**(22), 4870-4883.

Ostachowicz, W., Kudela, P., Krawczuk, M. and Zak, A. (2012), Guided Waves in Structures for SHM: The Time – domain Spectral Element Method, *John Wiley & Sons* , Chicester, United Kingdom.

Peng, H., Meng, G. and Li, F. (2009), "Modeling of wave propagation in plate structures using three-dimensional spectral element method for damage detection", *J. Sound Vib.*, **320**(4-5), 942-954.

Ramadas, C., Balasubramaniam, K., Joshi, M. and Krishnamurthy, CV. (2009), "Interaction of primary anti-symmetric Lamb mode with symmetric delaminations: numerical and experimental studies", *Smart Mater. Struct.*, **18**(8), 085011H.

Ramadas, C., Balasubramaniam, K., Joshi. M. and Krishnamurthy. C.V. (2010), "Interaction of guided Lamb waves with an asymmetrically located delamination in a laminated composite plate", *Smart Mater. Struct.*, **19**(6).

Rose, J.L. (1999), *Ultrasonic Waves in Solid Media*, Cambridge University Press, Cambridge, United Kingdom.

Rose, J.L. and Soley, L.E. (2000), "Ultrasonic guided waves for anomaly detection in aircraft components", *Mater. Evaluation*, **50**, 1080-1086.

Song, W.J., Rose, J.L. and Whitesel, H. (2003), "An ultrasonic guided wave technique for damage testing in a ship hull", *Mater. Evaluation*, **60**, 94-98.

Stewart, J.R., Gullerud, A.S. and Heinstein, M.W. (2006), "Solution verification for explicit transient dynamics problems in the presence of hourglass and contact forces", *J. Comput. Method. Appl. Mech. Eng.*, **195**, 1499-1516.

Veidt, M., Ng, C.T., Hames, S. and Wattinger, T. (2008), "Imaging laminar damage in plates using Lamb wave beamforming", *Adv. Mater. Res.*, **47-50**, 666-669.

Veidt, M. and Ng, C.T. (2011), "Influence of stacking sequence on scattering characteristics of the fundamental anti-symmetric Lamb wave at through holes in composite laminates", *J. Acoust. Soc. Am.*, **129**(3), 1280-1287.

Viktorov, La., Zubova, O.M. and Kaekina, T.M. (1965), "Investigation of Lamb wave excitation by the wedge method", *Soviet Physics-Acoustics*, **10**(4), 354-359.
Zhu, W., Rose, J.L., Barshinger, J.N. and Agarwala, V.S. (1998), "Ultrasonic guided wave NDT for hidden corrosion detection", *Res. Nondestruct. Eval.*, **10**(4), 205-225.